ACS Photonics

Article

pubs.acs.org/journal/apchd5

Miniaturized Sensing Probes Based on Metallic Dielectric Crystals Self-Assembled on Optical Fiber Tips

Marco Pisco,[†,⊥] Francesco Galeotti,[‡,⊥] Giuseppe Quero,[†] Agostino Iadicicco,[§] Michele Giordano,*[,∥] and Andrea Cusano*[,†]

[†]Optoelectronic Division, Engineering Department, University of Sannio, Benevento, Italy

[‡]Institute for Macromolecular Studies, National Research Council, Milano, Italy

[§]Department of Engineering, University of Naples "Parthenope", Naples, Italy

[∥]Institute of Composite Biomedical Materials, National Research Council, Naples, Italy

Supporting Information

ABSTRACT: We propose a novel fabrication process to realize optical sensing probes based on metal−dielectric crystals self-assembled on an optical fiber tip. The breath figure methodology has been adapted to work directly on nonconventional substrates, such as optical fibers, enabling the formation of regular and ordered metallo-dielectric crystals on optical fiber tips. Accurate morphological characterization was carried out to qualify the fabrication process. The reported results indicate that the proposed fabrication technique provides a method for rapid and cost-effective prototyping of photonic−plasmonic nanoprobes for sensing applications. To achieve this goal, we develop a technological platform via the addition of polymer−metal crystals onto the tip of a standard single optical fiber, which is able to support surface plasmon resonances in the near-infrared. A dedicated numerical tool was developed to study and analyze arbitrary subwavelength structures integrated on the optical fiber tip by taking into account finite-size effects. The numerical results are in good agreement with the observed experimental spectra and reveal that the fabricated sensing probes act as structured interferometers that are assisted by surface plasmon excitations at the metallo-dielectric interfaces. To prove the sensing capability of the proposed platform, refractive index measurements were carried out, revealing a sensitivity of up to 2300 nm/RIU, outperforming most plasmonic probes synthesized on optical fiber tips. The achieved performances, obtained using very small active areas, demonstrate the effectiveness of these self-assembled fiber-optic probes for label-free chemical and biological sensing applications.

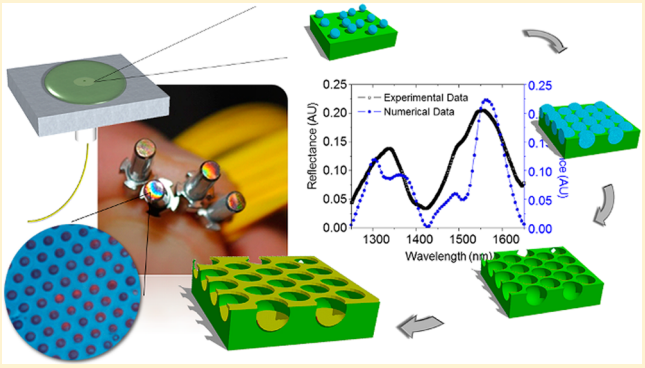

KEYWORDS: *breath figures, self-assembly, optical fiber sensors, sensing probes, optical fiber tip*

In recent decades, the development of sensors based on surface plasmon resonances (SPRs) for the detection of chemical and biological species has received considerable scientific attention. Several optical configurations have been proposed to exploit the properties of surface plasmons in different sensing applications and in more disparate sectors, such as medical diagnostics, environmental monitoring, and food safety.[1,2]

Surface plasmons are extremely sensitive to any local refractive index change occurring at the metal−dielectric interface. The excitation of an SPR leads to an increase in the light absorbance at the resonance condition, which in turn depends on the refractive index of the dielectric medium in the proximity of the metallic surface.[1,2] This dependence is exploited in various detection schemes for chemical and biological sensing applications, thus enabling the label-free detection of target molecules in real time and at very low concentrations.

To efficiently trigger the excitation of surface plasmons, traditional coupling schemes involve the use of prism couplers and diffraction gratings,[3] which are currently outperformed by miniaturized and integrated lab chip architectures and optical waveguides.[4]

Among them, SPR sensors based on optical fibers are particularly attractive by virtue of the intrinsic advantages associated with the use of fiber-optic technology. The challenge in exploiting fiber-optic SPR phenomena in optical fiber sensors arises from the difficulty of implementing an efficient and controlled coupling method for plasmonic excitation within the optical fiber. Despite these complications, a large number of

Received: November 15, 2013
Published: September 18, 2014

SPR fiber sensors have been demonstrated. Many excellent reviews covering this topic can be found in recent reports that have collected the latest and most relevant achievements.[4−6]

Essentially, in many optical configurations, the evanescent field of the light guided in an optical fiber is used to excite propagating surface plasmons in a thin metallic film covering a well-defined portion of the optical fiber along its axis. These optical configurations include cladding-removed optical fibers,[7,8] tapered fibers,[9,10] and U-shaped optical fibers,[11] all of which are coated with a thin metallic layer. These sensors often demonstrate excellent sensing performances in terms of sensitivity to the external refractive index (thousands of nanometers per refractive index unit (RIU)), but they typically suffer the disadvantages of fragility and large surface area, requiring a larger number of target molecules bonded to the fiber surface to provide a given refractive index change. Recently, the fragility limitations of these fibers have been successfully addressed through the use of various types of fiber gratings[12] or specialty fibers, such as D-shaped fibers[13] and photonic crystal fibers.[14,15] However, these sensors still suffer the disadvantage of having large active areas, which in turn limits the detection accuracy in terms of biomolecule concentration.

An exciting method for the achievement of fiber-optic plasmonic probes with reduced active areas involves the use of optical fiber tips as technological substrates for the realization of functional sensing nanoprobes with unique features in terms of compactness, intrusiveness, and overall performances that are suitable for use as ex vivo and in vivo biosensors.

The simplest realizations of optical fiber tip SPR are still based on fiber tapering and cladding removal. Grunwald et al. proposed an SPR sensing element that consisted of a single-ended tapered optical fiber coated with a 50 nm gold layer.[16] Similarly, to obtain an SPR fiber tip sensor, Suzuky et al. removed the cladding of a multimodal optical fiber over 20 mm long, deposited a gold layer around the core using thermal evaporation, and deposited a silver metal layer on the end of the fiber to form a mirror.[17]

More interesting and compact examples of fiber-optic tip SPR sensors involve the integration of metallic or metallic−dielectric nanostructures supporting localized SPRs (LSPRs). These sensing configurations are highly miniaturized, down to the micrometer scale. They enable the engineering of light confinement and, therefore, provide sensitivity to local optical changes using a design that takes advantage of the many degrees of freedom exhibited by these structures.

LSPRs are nonpropagating resonant surface plasmons that can be excited on metal nanoparticles or around nanoholes in metal films.[2] Furthermore, LSPRs are highly sensitive to the size, distribution, and shape of the nanoparticles and can be used to precisely tailor devices for specific applications.[18]

Various metallic nanostructures, such as ordered apertures in metallic films, metallic nanopillars, and nanorods attached to optical fiber ends, have been proposed and experimentally validated for compact and label-free biochemical detection.

Lin et al. reported an LSPR biochemical sensor based on the transmission spectra of an ordered array of metallic nanodots fabricated on an optical fiber tip using electron beam lithography (EBL).[19,20] Similarly, Dhawan et al. demonstrated optical sensors based on SPRs and LSPRs associated with metallic nanostructures synthesized on an optical fiber tip using a focused ion beam (FIB).[21,22] Hybrid metallo-dielectric nanostructures supporting LSPRs have also been fabricated directly on a single-mode fiber tip using a modified spin-coating method combined with EBL nanotechnology.[23] Sensitivities of a few hundred nanometers per RIU are typically achieved using LSPR-based sensing configurations.

The fabrication routes employed for the construction of these sensing probes mainly rely on the use of well-understood nanofabrication tools and lithographic procedures that are commonly used for planar substrates and have been adapted and modified to work correctly on nonconventional substrates, such as optical fiber tips.[24,25]

However, these fabrication techniques require expensive instruments, such as EBL and FIB, resulting in time-consuming and expensive processes, which are valuable for prototype demonstrations but unsuitable for the mass production of functional nanoprobes.

Alternative fabrication routes often feature two distinct phases: the first phase generates the photonic−plasmonic crystal in a planar configuration using well-known technologies and procedures, and the second stage aims to transfer the crystal to the fiber tip.[25] Following this type of approach, well-arranged nanostructure arrays on fiber tips were reported by Smythe et al.[26,27] They described a transfer technique in which various metallic patterns have been individually defined using EBL and then moved to the optical fiber tips. Next, to increase the production throughput, the same authors developed another technique to create metallic nanostructures by embedding and sectioning a metalized array of epoxy nanoposts using an ultramicrotome.[28] These transferred structures on fiber tips have been used for all-fiber LSPRs and surface-enhanced Raman spectroscopy (SERS)-based sensing devices.

As a drawback, all of these fabrication procedures inevitably concentrate the procedure complexity in the transfer step, which can be considered the crucial step that determines the final fabrication yield and the performance of the final device.

The use of self-assembly methodologies specialized to operate directly on optical fiber tips seems to be a promising approach for overcoming fabrication issues, such as the use of expensive nanotechnologies and the difficulty of realizing high throughput.

The autonomous organization of micro- and nanostructures in regular ensembles on optical fiber tips is the key to obtaining ordered patterns on a large number of optical fibers simultaneously. However, the self-assembly processes successfully demonstrated for large planar substrates often fail when they are required to operate on confined substrates, such as fiber tips. For this reason, only a few attempts, mostly based on nanoparticle self-assembly, have been reported in the literature.

Stoddart et al. evaluated the use of a simple "dip and dry" method for producing periodic nanoparticle arrays on the tips of optical fibers, resulting in a combination of mono- and multilayer zones and inhomogeneous fiber coverage.[29] Yap et al. arranged gold nanoparticle clusters on optical fiber tips using an electrostatic self-assembly approach guided by a block copolymer template and proposed their use for sensors based on SERS.[30] Although this method yielded ordered clusters on a planar substrate, an attempt to reproduce the process on fibers gave rise to close-packed but unordered gold clusters due to the insufficient ordering of the polymer template. Andrade et al. decorated a fiber tip with Ag nanoparticles using a layer-by-layer approach for SERS biosensing.[31] This approach, which requires the chemical modification of the fiber tip surface, is capable of producing 1 to 5 overlapping layers of nanoparticles separated by an organic spacer. The lateral arrangement of the

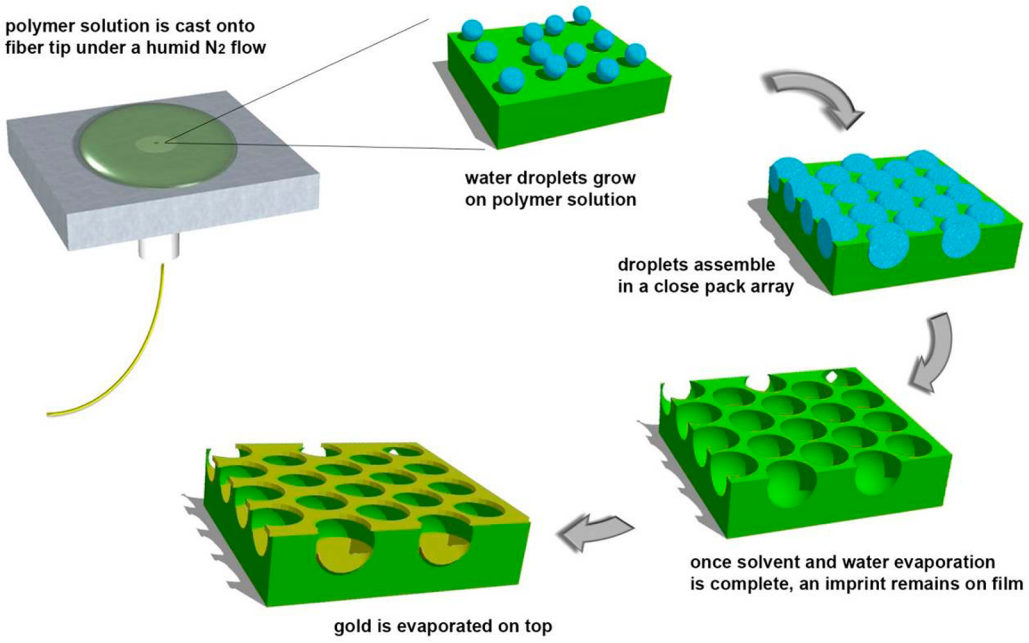

Figure 1. Schematic overview of the fabrication process.

nanoparticles in each plane cannot be controlled. Yan et al. etched a cavity on one fiber facet and filled this cavity with a colloidal dispersion of nanoparticles in PMMA, yielding a photonic crystal.[32] In this study, the nanoparticle assembly is synthesized via the slow evaporation of the solvent; therefore, only multilayers can be obtained.

All of these studies reveal that, although the self-assembly approach is potentially attractive for patterning optical fibers, synthesizing metallic dielectric crystals via assembling solid objects in a highly ordered fashion directly on a fiber tip is complicated. Hence, alternative fabrication procedures should be explored.

With this goal, we moved to an entirely different approach that does not require the use of nanoparticles. Our idea was to exploit the self-assembly phenomenon known as breath figure (BF) formation and to realize it directly on the fiber tip.[33] The BF method is capable of producing thin polymeric films with micrometer cavities arranged in a hexagonal fashion with the following benefits: (i) a single-step approach, (ii) no need for lithographic processing, (iii) duration of a few seconds, and (iv) the use of very simple and accessible laboratory equipment.[34−36] Indeed, this approach uses a templating method in which the template consists of an ordered array of water droplets that can be removed through simple evaporation, which is an indisputable advantage with respect to most of the other known templating techniques, where the templates must be removed after the fabrication of the porous films, and in most cases, they are not easily prepared or removed. Compared to the nanoparticle approach, this assembly is produced at the polymer/air interface, overcoming all of the problems related to the interaction of the assembled objects with the substrate, which is a critical requirement for perfectly packed nanosphere layers.

In this paper, we present recent results on the use of the BF approach in the synthesis of ordered metallo-dielectric structures on optical fiber tips. In particular, we report details of the fabrication process supported by a wide morphological analysis and discuss the related principle of operation through numerical and experimental analysis. Finally, the functionality of the probes for sensing applications is demonstrated.

RESULTS AND DISCUSSION

Breath Figures on Optical Fiber Tips. The strategy for the fabrication of periodic structures on optical fibers initially involves the coating of the fiber tip with a microporous polymer film via the BF technique. This self-assembly approach allows for the preparation of honeycomb-like arrays on the micrometer scale with a high degree of order despite the simplicity of the process. The mechanism of BF formation has been described in detail by several authors and will be recalled briefly here.[37−39] The process relies on the precipitation of a polymer around condensed water droplets, initiated by the rapid evaporation of a polymer solution in a humid environment. Its salient stages are depicted in Figure 1. In the initial stage, the endothermic evaporation of the solvent results in a decrease of the system temperature, thus triggering water condensation. Once a droplet of water has nucleated on the polymer solution, it grows at the expense of the vapor in the surrounding atmosphere. During this stage, the growing droplets auto-organize at the polymer solution/air interface into a close hexagonal arrangement. Once the film returns to ambient temperature, the condensed water and residual solvent evaporate, leaving behind a honeycomb structure. When the process is adequately controlled and the key parameters (polymer concentration, solvent type, evaporation rate, and relative humidity) are accurately adjusted, the morphology of the final film, i.e., the degree of order, distribution, and size of the cavities, is fairly controllable.

Even though the applicability of the BF approach in the fabrication of both metallic disk arrays and metallic meshes has already been established,[40,41] this report is the first study, to the best of our knowledge, that makes use of BFs as a tool for synthesizing self-assembled metallo-dielectric periodic structures on the tips of standard, single-mode optical fibers.

To achieve this goal, the standard setup, which is normally utilized for making honeycomb films on glass or silicon

dx.doi.org/10.1021/ph500126v | ACS Photonics 2014, 1, 917−927

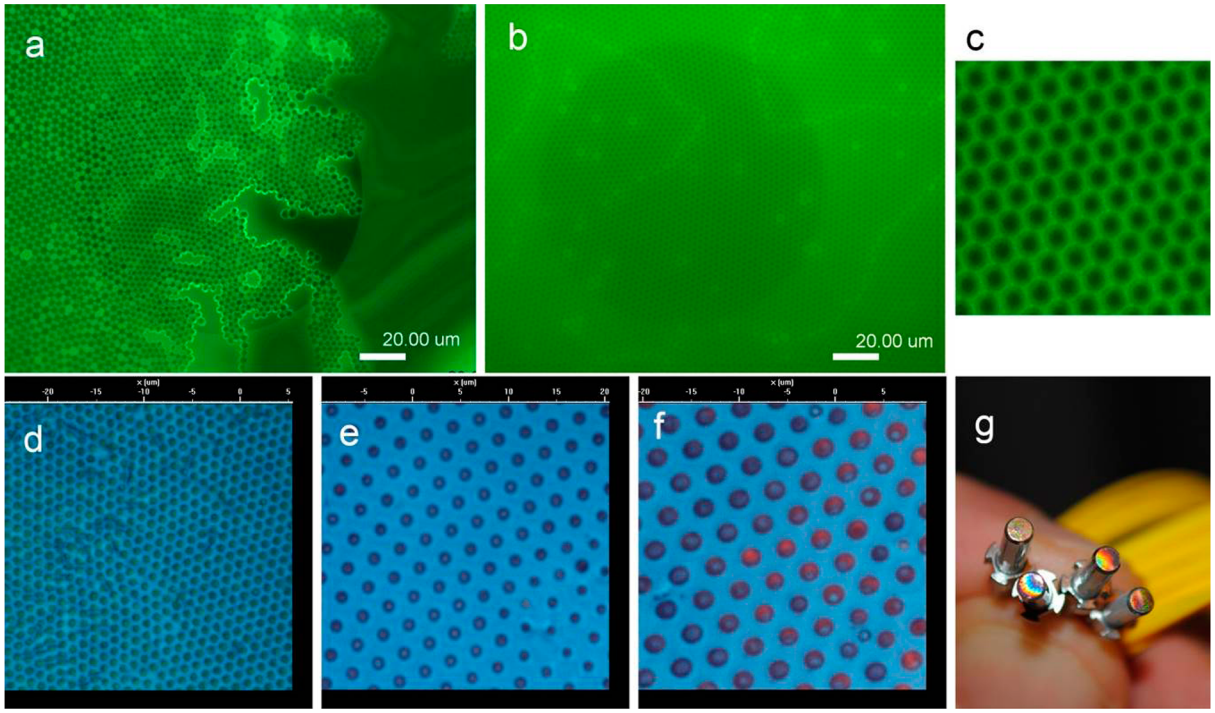

Figure 2. (a, b) Fluorescence microscopy images of patterned polymer film on the fiber, showing incomplete patterning due to low water condensation (a) and full honeycomb coverage (b). The darker round area in the center of each image corresponds the fiber facet. (c) Confocal microscopy image of a magnified portion of (b) taken near the center of the fiber (side 20 μm). (d–f) Confocal microscopy images of the patterned fiber after Au layer deposition, showing the increase in the pore size obtained by reducing the N_2 flow rate (side 30 μm). (g) Picture of the fiber-optic prototypes, showing iridescent colors.

substrates, must be adapted to work with nonconventional substrates, such as optical fibers. The main issue to be addressed is the fiber tip size: 125 μm in diameter for a standard single-mode fiber. Typically, highly regular BF arrays are obtained by spreading a few droplets of the polymer solution over a flat surface of 1–5 cm^2. Unfortunately, the fiber tip is too small for such an approach. To overcome this issue, the optical fiber was embedded in a ceramic ferule with a diameter of 2.5 mm (similar to the ferule used in standard fiber connectors FC/PC) and then accurately polished. This modified fiber tip offers a larger surface compared with the bare fiber, resulting in easier handling during both the fabrication process and the operative stage of the final device.

Although we have experimentally shown that it is possible to prepare BF films directly on fiber tips modified in this way, the reproducibility of this approach is rather poor due to the low casting volume (4 μL) and, consequently, quicker evaporation of the polymer solution. Therefore, the use of a holder that increases the deposition surface is recommended. For this purpose, an Al holder with dimensions of 20 × 20 × 8 mm was designed to fit the ceramic ferule external diameter, thus preventing any solvent leaking, so that the polymer solution can be easily drop cast over an area of approximately 1 cm^2 (see initial sketch in Figure 1). Because the fiber is placed exactly in the center of the holder, only the central portion of the film is deposited on it, which also overcomes the problem of poor pattern homogeneity that is usually encountered on the edges of BF films.[42] Moreover, this approach is, in principle, suitable for patterning more than one fiber at the same time by simply designing a multislot Al holder and by casting a wider film. The Al holder was precooled by placing it on a cold stage maintained at a temperature of +10 °C and removed immediately before starting the film deposition. In fact, based on the high thermal conductivity of the metal substrate compared to glass or other typical substrates for BFs, the evaporation-induced cooling of the polymer solution is mainly dispersed through the Al substrate, resulting in poor water condensation (Figure 2a). For this reason, the precooling step is required to promote efficient water condensation on the evaporating film and, consequently, the BF formation (Figure 2b).

Films were prepared by drop casting with a micropipette directly on the fiber/holder assembly, depositing 50 μL of CS_2 solution (4 mg/mL) of a fluorinated fluorescent dye-terminated linear polystyrene, which we had already described as a good candidate for producing highly ordered BF structures.[43] The refractive index of this polymer is 1.58 (at a wavelength of 550 nm, measured using ellipsometry), which is consistent with the tabulated data for standard polystyrenes.[44] To speed up the solvent evaporation and promote water condensation, a flux of moist nitrogen (75% RH at 25 °C) was directed toward the fiber. The solvent completely evaporated in a few seconds, living an opaque film on the holder and fiber surface, which shined in bright, iridescent colors, indicating a periodic variation in the refractive index (air holes/polymer walls) throughout the surface of the film (Figure 2g). Using the fluorescence emission of the polymer, we were able to rapidly check the quality of the patterns formed on the fiber using fluorescence microscopy (see Figure 2a–f). Once the BF process was complete, the fiber was carefully detached from the holder, and its tip retained a portion of the honeycomb film.

Because all of the other external parameters (nitrogen temperature and humidity), as well as those related to the preparation procedure (solvent, polymer concentration, and

dx.doi.org/10.1021/ph500126v | ACS Photonics 2014, 1, 917–927

casting volume), remained constant, control of the pore size was achieved by varying the flow of the humid nitrogen directed at the fiber tip. Because the pores are formed by condensed water droplets, which act as the template, the size of the droplets controls the size of pores. For example, to produce a smaller porosity, the condensed water droplets should be small; therefore, the solvent evaporation time should be faster, so less time was allowed for the droplets to grow. This growth can be controlled in two ways: regulating the thickness of the casting solution using a blade deposition system or adjusting the flow rate of the humid nitrogen directed at the sample.[42] In a very recent publication, Yamazaki et al. reported a theoretical approach showing that it is possible to predict the water droplet growth time in a BF system.[45]

Even though a flow rate/size dependence was not accurately determined at this stage of the study, by varying the nitrogen flow between 320 and 220 L/h, it was possible to regulate the solvent evaporation time between 5 and 20 s, respectively, which produced honeycomb arrays with external diameter ranging from 1.0 to 2.5 μm and lattice period ranging from 1.5 to 4.0 μm, as shown in Figure 2d–f.

In Table 1 we report the pattern fabrication results obtained by varying the casting procedure, on the basis of the resulting lattice period (see Figure S1 in the Supporting Information).

Table 1. Variation of Lattice Period with Casting Procedure for Different Patterns Prepared on the Optical Fiber

procedure	moist N_2 flow rate [L/h]	average lattice period [μm]	standard deviation (n of samples)
1	320	1.7	0.14 (9)
2	300	2.6	0.16 (10)
3	250	3.2	0.18 (3)
4	220	3.9	0.11 (4)

Once the optical fiber facet was covered with the polymeric honeycomb structure, the quality of the pattern in the center of the fiber was checked using fluorescence microscopy, so that well-ordered and defect-free arrays with the desired dimensions were selected for the following step. The second fabrication step consisted of the vacuum thermal evaporation of a thin layer of Au over the tip. To achieve this goal, the fiber was placed in a vacuum evaporation chamber and 30 to 40 nm of Au was deposited on top. Using this two-step procedure, prototypes consisting of single-mode optical fibers end-coated with ordered, metal–dielectric crystals have been successfully synthesized (Figure 1, final sketch).

Morphological Characterization. The complete morphological characterization of two representative samples (1 and 2) obtained by procedures 2 and 4, respectively (see Table 1), is reported and discussed.

Figure 3a contains a scanning electron microscope (SEM) top view image of sample 1 in which a ceramic ferule (2.5 mm diameter) with smoothed edges can be observed. The pattern is poorly visible. In Figure 3b and c, we show a magnified SEM image and an atomic force microscope (AFM) image of the structure, respectively, allowing for accurate study of the topography of the patterned region. By analyzing the images, the key parameters of the periodic pattern of holes were measured, revealing a lattice period and hole diameter of 2.67 and 0.95 μm, respectively. The relative standard deviations (% RSD) of both geometrical parameters were estimated to be 1.3% and 3.2%, respectively. Additionally, the AFM profile shown in Figure 3d enabled the measurement of the mean pore depth, which was 1.78 μm (RSD of 3.5%). Finally, to investigate the overall structure thickness and uniformity, we first removed the polystyrene on half of the ceramic ferule using an excimer laser (operating at a wavelength of 248 nm) and then measured the structure height using AFM. The laser fluence and repetition rate were selected to ablate the polystyrene layer without damaging the ceramic surface. An SEM top view image of the carved sample is shown in Figure 3e, where the treated region is clearly evident. In Figure 3f and g, we show an AFM image and AFM profile of the treated region, revealing a polystyrene height of 2.5 μm with a relative standard deviation of 2.3%. The polystyrene thickness is higher than the hole height, revealing the presence of a uniform polystyrene undercoating, which is estimated to be 0.72 μm thick.

A similar morphological characterization was performed on sample 2. Figure 4a and b show the AFM topography and vertical profile of the patterned region, respectively. The lattice period, hole diameter, and hole depth were measured and found to be 3.76, 1.71, and 3.41 μm, respectively.

The reported results demonstrate the ability of the proposed method to synthesize regular and ordered polymeric templates

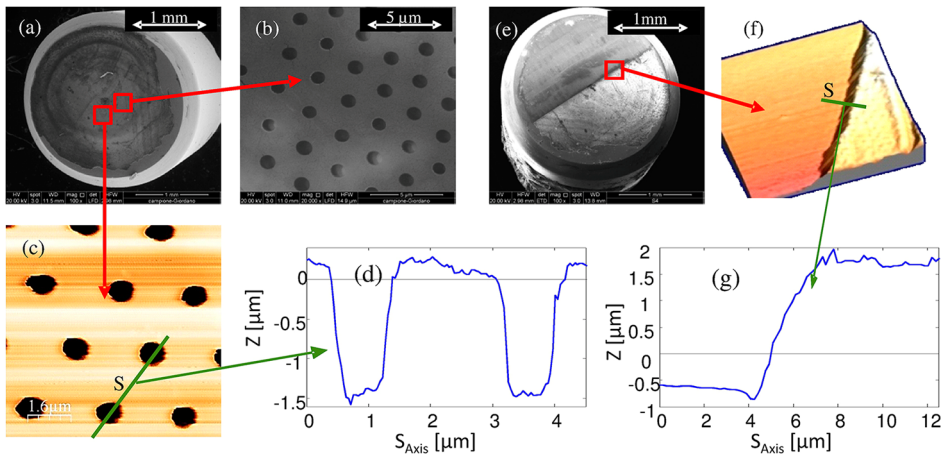

Figure 3. Morphological characterization of sample 1: (a) SEM top view; (b) magnified SEM image; (c) AFM topography; (d) z profile vs S line in (c); (e) SEM top view after half of the laser removal; (f) AFM topography of the laser-treated-region edge; and (g) z profile vs S line in (f).

dx.doi.org/10.1021/ph500126v | ACS Photonics 2014, 1, 917–927

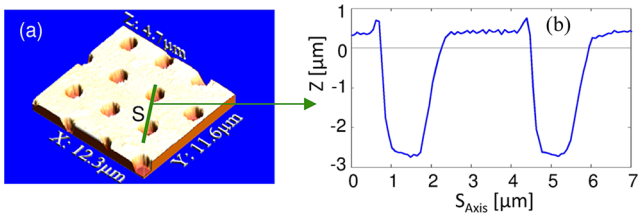

Figure 4. Morphological characterization of sample 2: (a) AFM topography and (b) z profile vs S line in (a).

on the tips of standard, single-mode optical fibers, providing a method for the simple production of fiber-optic probes for specific applications via the judicious integration of functional overlays onto the self-assembled pattern.

We evaluated the packing of pores on the fiber tip by applying Voronoi tessellation to the microscopy images, obtaining a value for the entropy of conformation (S) of 0.15 (see Supporting Information).[46] Considering that for perfect hexagonal packing $S = 0$ and for random packing $S = 1.71$, we can conclude that our patterns are very close to perfect hexagonal packing with a small number of defects.

Numerical and Experimental Spectral Analysis. Spectral reflectance measurements were carried out via a common measurement setup involving a 3 dB 1 × 2 coupler connected to a broadband light source (covering the wavelength range 1250−1650 nm), the fiber probe, and an optical spectrum analyzer. In Figure 5a, we show the experimental reflectance spectrum (black line) of sample 1, revealing a broadband peak centered at approximately 1400 nm.

To investigate the physics underlying the observed spectrum, we performed a numerical analysis using the geometrical features obtained from the morphological characterization reported in the previous section. The structure realized is numerically reconstructed in the form of a thin polystyrene uniform layer beneath the BF pattern, as schematized in Figure 5b. The entire structure is assumed to be covered by a conformal thin film of gold.

To numerically retrieve the reflectance of the photonic crystals, a common approach requires the calculation of the scattering parameters of a slab that consists of the unit cell with periodic boundary conditions.[47−49] Nevertheless, this approach does not yield a faithful representation of the photonic structure under investigation (see the numerical section in the Supporting Information). To improve the predictive capability of our analysis, we developed a novel numerical model that considers a Gaussian-like mode as the input light and takes into account the finite size of the periodic structure, including a limited number of unit cells.

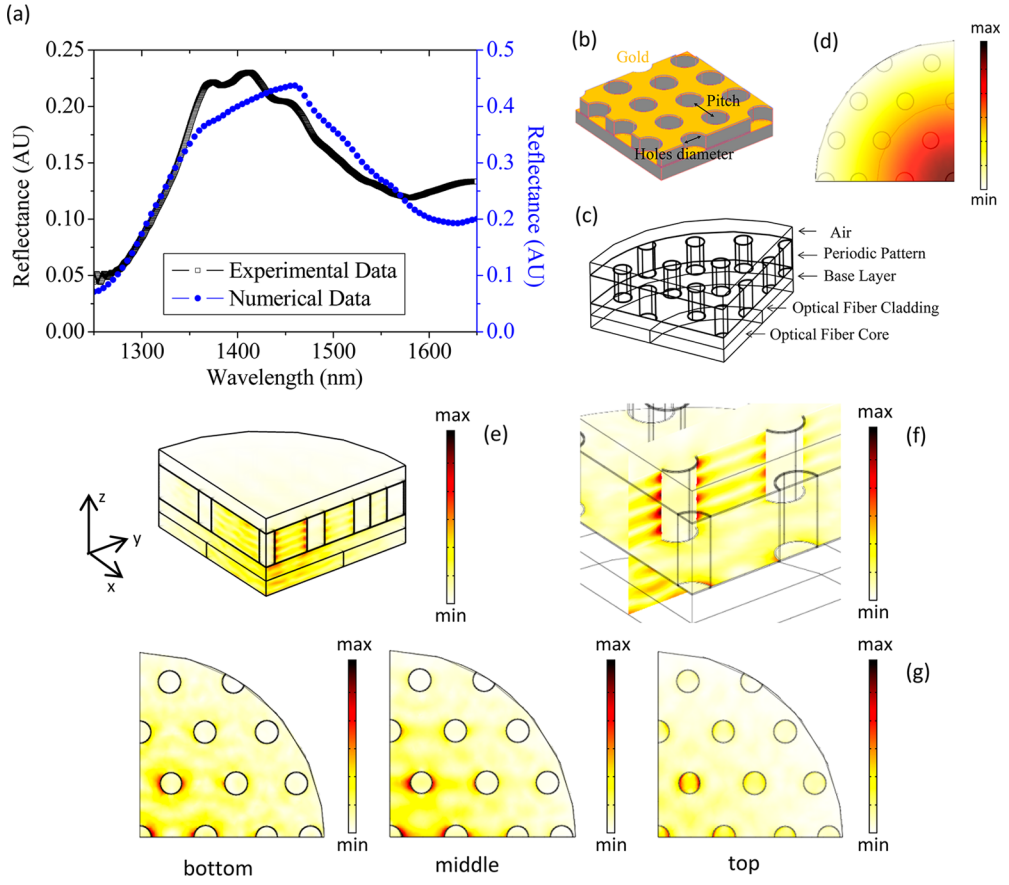

Figure 5. (a) Numerical reflectance retrieved by the optical fiber based model in comparison with the experimental reflectance of the sample 1. (b) Schematic top view of the hybrid metallo-dielectric structures. (c) Computational domain for the optical fiber based model. (d) Normalized electric field distribution of the input light source superimposed on the periodic pattern of the optical fiber. (e) Lateral view of the normalized electric field distribution at 1400 nm. (f) Normalized electric field distribution at 1400 nm along two orthogonal slices in the xy and yz planes. (g) Top view of the normalized electric field distribution at 1400 nm in a slice at the bottom (gold disks), in the middle, and at the top (holes in metal film) of the metal−dielectric structure.

dx.doi.org/10.1021/ph500126v | ACS Photonics 2014, 1, 917−927

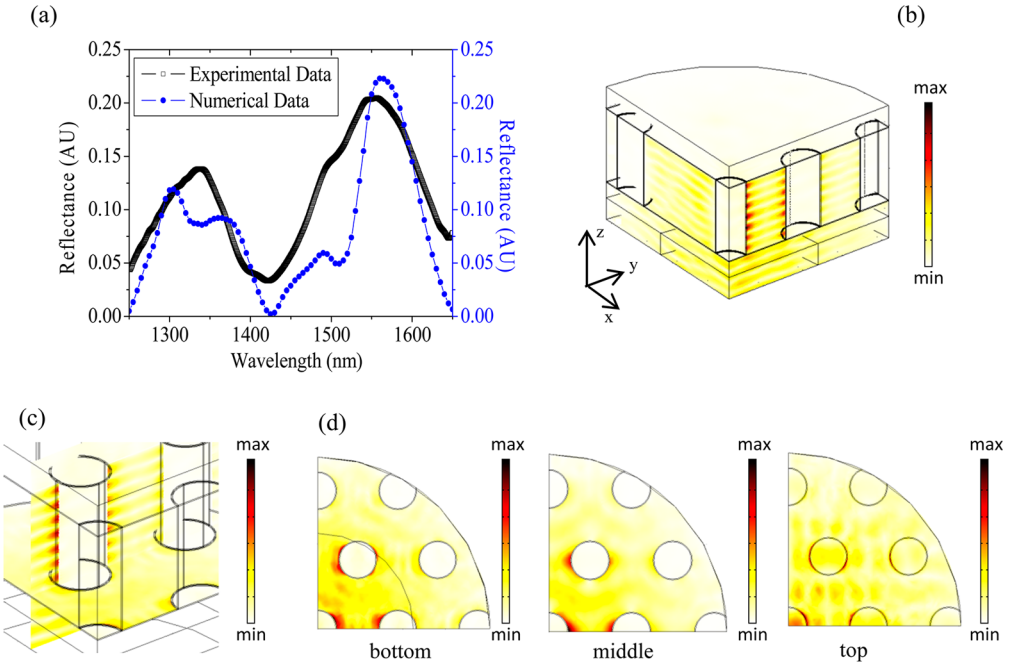

Figure 6. (a) Numerical and experimental spectra of the sample 2. (b) Lateral view of the normalized electric field distribution at 1550 nm. (c) Normalized electric field distribution at 1550 nm along two orthogonal slices in the *xy* and *yz* planes. (d) Top view of the normalized electric field distribution at 1550 nm in a slice at the bottom (gold disks), in the middle, and at the top (holes in metal film) of the metal−dielectric structure.

The corresponding computational domain, shown in Figure 5c, involves a thin slice of optical fiber composed of a core with a diameter of 9 μm and a reduced cladding with a diameter of 16 μm radially terminated by a perfect electric conductor. The physical and geometrical features of this modified optical fiber have been chosen to ensure single-mode propagation with a Gaussian-like mode distribution (see the Methods section for further details). The metallo-dielectric structure to be simulated is drawn on the optical fiber tip and followed by a layer of air, which represents the surrounding medium. The dimensional parameters used for the simulation are hole diameters of 0.95 μm, pitch of 2.67 μm, hole depths of 1.78 μm, base layer height of 0.72 μm, and gold thickness of 33 nm. Figure 5d shows the resulting input mode field distribution superimposed on the computational domain.

In Figure 5a, we show the numerical reflectance spectrum (blue line) retrieved using the "optical fiber based model" compared with the experimental results (black line), demonstrating that numerical and experimental data agree well. The only appreciable difference is in the maximum reflectance values, 25% and 50% for the experimental and numerical data, respectively. This mismatch can be explained considering the unavoidable fabrication defects with respect to the ideal structure considered in the numerical analysis.

In Figure 5e, we show the electric field distribution at 1400 nm, which is representative of the entire investigated spectral range. At first glance, the normalized electric field appears quite similar to that observed in a two-beam interferometric structure, featuring sinusoidal behavior along the propagation direction. However, due to the structured and inhomogeneous nature of the optical cavity, remarkable differences are evident in the patterned holes of the self-assembled crystal, where significant field localization can be clearly observed (see Figure 5f) at the interfaces between the thin layer of gold and the surrounding dielectric. To better evaluate the nature of this field localization, we show top views of traversal slices from the bottom, middle, and top of the patterned region in Figure 5f. As can be observed, the enhancement of the electric field around the holes resembles the typical dipolar field distribution associated with the excitation of an LSPR in a gold disk (or ring).[50]

Moreover, this behavior can be observed in the gold disks at the bottom of the metal−dielectric structure, around the gold rings in the middle of the polystyrene substrate, and on the rims of the holes in the upper part of the gold layer (see Figure 5g). In addition, the field enhancement extends along the vertical metallic sides of the holes, revealing the presence of surface plasmon waves that "propagate" along the fiber axis in the metallo-dielectric structure, similar to the behavior observed by Nuzzo et al.[51]

These considerations lead us to envision a complex interplay occurring between the classical optical interference mechanism and the plasmonic excitation occurring at the metallic interfaces. Nonetheless, although the electric field distributions indicate the presence of propagating and localized plasmons, the numerical and experimental spectral characteristics do not contain spectral lines clearly attributable to plasmonic effects, most likely due to finite size effects. With the exception of small bumps on the experimental spectrum, the shape of the reflectance can be considered dominated by two-beam interference; the spectral separation of the minima is consistent with the size of the structured cavity.

A similar analysis was carried out for sample 2, whose experimental reflectance is shown in Figure 6a. The hole diameters, pitches, and depths are assumed equal to their respective mean values that were determined from the morphological characterization (1.71, 3.76, and 3.41 μm), and the gold thickness is 40 nm, whereas for the polystyrene undercoating, due to the lack of a measurement, we used the same height of 0.72 μm that was measured in sample 1. It should be emphasized that the spectrum is minimally affected

dx.doi.org/10.1021/ph500126v | ACS Photonics 2014, 1, 917−927

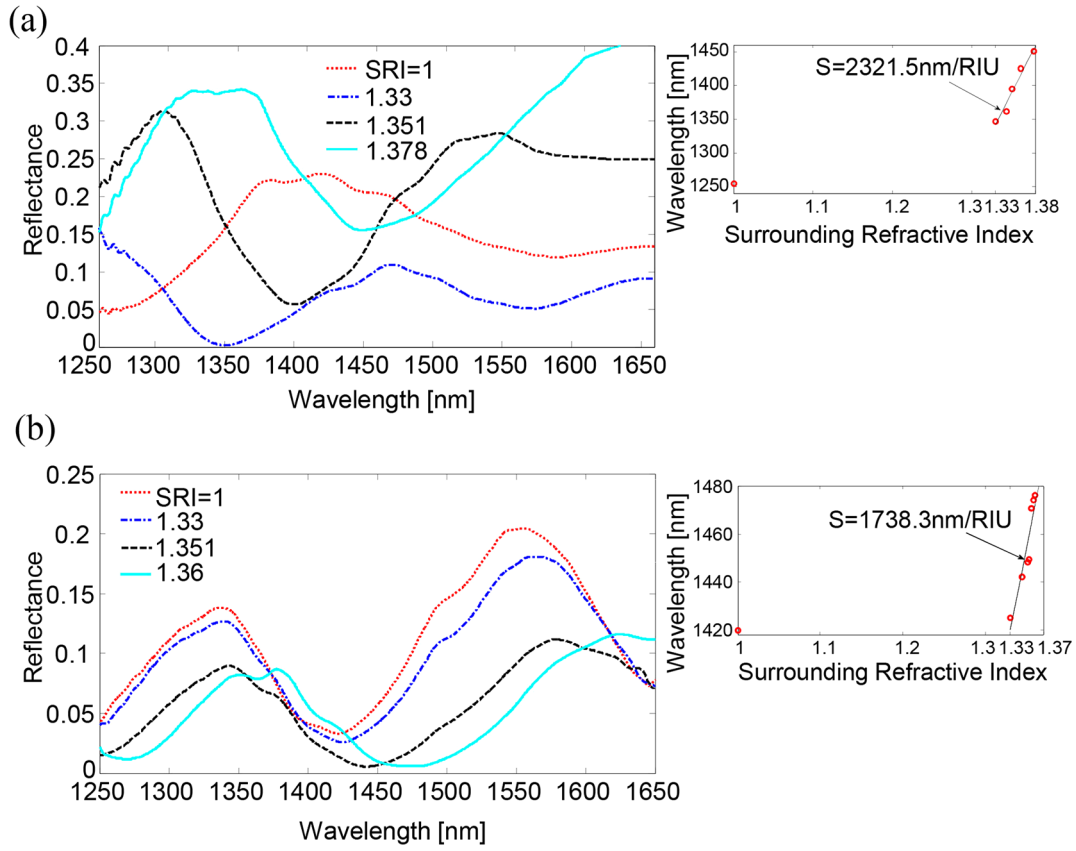

Figure 7. (a) Experimental reflectance spectra of sample 1 as a function of the SRI (inset shows the wavelengths of the reflection dip vs SRI) and (b) experimental reflectance spectra of sample 2 as a function of the SRI (inset shows the wavelengths of the reflection dip vs SRI).

by the base layer thickness because of the low refractive index contrast between silica and polystyrene.

The numerical and experimental reflectances are shown in Figure 6a, where good agreement can be observed. Moreover, the analysis of the electric field distribution confirms our conjecture of a plasmonic-assisted optical interferometer. In Figure 6b and c, the normalized electric field distributions are shown at 1550 nm, which is representative of the investigated wavelength range, both from a lateral view and along two orthogonal slices in the *xy* and *yz* planes, respectively. From the lateral view in Figure 6c, the sinusoidal behavior of the electric field intensity along the fiber axis can be observed, while the slices in Figure 6d (orthogonal to the fiber axis) have been selected at the bottom (gold disks), in the middle (gold rings), and at the top (holes in metal film) of the metal dielectric structure to better highlight the electric field enhancement around the conformal gold layer. Additionally, the optical interferometric interaction in the structured cavity can be considered the dominant feature of the observed reflectance spectra.

Sensing Features: Refractive Index Sensitivity. Because the physical mechanism of the probes relies on the interplay between interferometric and plasmonic effects, significant refractive index sensitivity could be expected, especially based on the field enhancement occurring at the metal interface.

To assess the sensitivity of the fabricated samples to the surrounding refractive index (SRI), the optical fiber probes were immersed in different liquids with known refractive indexes, and the corresponding reflectance spectra were measured. In Figure 7a, the spectra of sample 1 for different SRIs are shown. The main effect is a significant red-shift of the overall spectrum combined with a modification of the reflectance amplitude and fringe visibility. By evaluating the wavelength shift associated with the reflectance minima as a function of the SRI, an impressive sensitivity of 2300 nm/RIU can be inferred over the refractive index range of 1.33−1.378.

The same procedure was also carried out for sample 2. The reflectance spectra as a function of the bulk SRIs are shown in Figure 7b. The spectra still red-shift with increasing SRIs, but a decrease in the reflectance values can be observed. The resulting sensitivity is 1738.3 nm/RIU in the refractive index range of 1.33−1.36.

For both samples, the SRI sensitivity results decrease when air is used as the surrounding medium, while it significantly increases for higher refractive indexes.

This behavior matches the sensitivity curves exhibited by most SPR devices,[3,52] whereas a two-beam interferometer would have a linear sensitivity to the SRI[53] (supposing that the change in the refractive index of the holes leads to a linear variation in the optical cavity path under the effective medium approximation in a dielectric mixture).[54] Nonetheless, the intensity changes observed in Figure 7a and b are consistent with the amplitude changes observed in LSPR-based devices.[52] A clear understanding of the interplay between the different optical effects arising in the structured cavity is currently ongoing and needed to provide useful insight into the physical mechanisms involved, as well as the design criteria for specific applications.

Although a complete understanding has not yet been attained, basic considerations of the experimental data indicate

that the interplay between the different effects provides sensitivity values typically observed in SPR devices involving large metallic areas.[4] In our case, these extremely high sensitivity values are achieved with active regions (fiber tip area 0.012 mm^2) typically used for LPSR devices that have sensitivity values that do not exceed a few hundred nm/RIU.[2,4]

The achieved sensitivity results are significant when compared with previous LSPR-based fiber tip probes.[19−23] Indeed, in our sensing probes, in spite of the low *Q*-factor at the reflection dip (lower than 15 for both samples), the obtained sensitivities to the SRIs are very high, especially if we take into account the small active area involved. For instance, the hybrid, metallo-dielectric nanostructures on a single-mode fiber tip give rise to LSPR devices with an SRI sensitivity of 125 nm/RIU.[23] In the same way, an ordered array of gold nanodots on a single-mode fiber tip proposed by Lin et al.[20] demonstrated an SRI sensitivity of 195.72 nm/RIU. A slightly higher sensitivity (533 nm/RIU) was demonstrated by Dhawan et al. by exploiting an array of subwavelength apertures on the tip of gold-coated multimode fibers.[21]

The comparison of our sensing performances with non-localized SPR-based sensors is also indicative. To achieve this goal, we consider the performances of SPR sensors recently reviewed by B. Lee et al.[5] and found that several SPR optical configurations that exhibit high sensitivities (ranging from 1600 up to 3000 nm/RIU) are based on optical fiber cladding removal and the subsequent deposition of single or multiple layers of metal coatings. In all of these configurations, the involved active areas range from approximately 6 up to 45 mm^2. Additionally, SPR sensors based on fiber gratings[12] or specialty fibers[13−15] exhibit large active areas, and the sensitivities are typically lower than 1000 nm/RIU.[4,5] Similarly, by examining the table containing the performances of SPR-based sensors reviewed by S. Roh et al.,[4] it is possible to notice the impressive sensitivity of 30 000 nm/RIU obtained using a nanostructured sensor in a Kretschmann configuration with a sensing area up to 2 cm^2.

It is useful to note that, when dealing with sensing platforms for label-free biosensing, the active sensing area is a very important parameter because it determines the performances of the final device in terms of the limit of detection. In many biorecognition applications (i.e., drug resistance recognition and early detection of cancer pathologies, pathogen agents, and infections), very low concentrations of the target biomolecules must be detected. For these applications, a given local refractive index change (on the sensor surface) is provided by a smaller number of bound biomolecules if biosensors with reduced sensing areas are used.[55]

Another remarkable advantage of the proposed sensing probes is represented by their low-temperature cross-sensitivity, as demonstrated by experimental measurements (also reported in the Supporting Information) carried out by changing the temperature of the surrounding air from 20 °C to 40 °C. As a result, a very small spectrum shift of approximately 1.4 nm for a temperature variation of 20 °C was obtained.

Definitively, we would like to emphasize that our fabricated sensing probes offer valuable sensing features exploitable for label-free chemical and biological sensing applications. Nevertheless, improvements of the sensing properties of the fabricated sensing probes are still desirable, especially in terms of shape and width of the obtained spectral features. A low *Q*-factor in fact limits the accuracy of the wavelength shift measurements, and the scarcely regular shape of the spectra may lead to a lack of resolution for sensing small refractive index changes.

We note that, at this stage, no attempts have been made to optimize the platform in terms of sensing performance, but it could be expected that, by exploiting the high number of parameters ruling the spectral response of the composite metallo-dielectric structures, further optimization routes exist (see the section "Trends for device design" in the Supporting Information).

CONCLUSION

In this work, we demonstrated a fabrication process that enables the integration of metallo-dielectric crystals directly onto optical fiber tips using a self-assembly approach. The fabrication technique relies on the use of the BF method operating directly on optical fiber tips by adopting a modification of the procedure. Regular and ordered, self-assembled polymeric patterns can be easily integrated on the tips of standard, single-mode optical fibers, which act as a template for successive depositions of functional materials that are able to confer advanced functionalities to the final device.

The effectiveness of the proposed process has been confirmed through the realization of specific optical fiber platforms based on the integration of hybrid metallo-dielectric crystals onto optical fiber tips. The miniaturized fiber tip devices were composed of a thin self-assembled polystyrene layer patterned with a hexagonal lattice of holes. The polymeric template was also covered by a conformal nanolayer of gold. Specifically, we selected gold as a functional material to confer plasmonic features and to exploit them for sensing applications.

A deep morphological analysis, carried out via SEM and AFM, confirmed the ability of the self-assembly process to create well-ordered, self-assembled lattice structures directly on the optical fiber tips. These structures were characterized by an entropy of conformation as low as 0.15, indicating that the organization is very close to perfect hexagonal packing. The quality of the order reached by this approach is comparable to that obtainable by lithographic nanofabrication and exceeds every pattern realized so far on optical fiber tips through self-assembly techniques.[29−32] The developed method provides a simple and cost-effective fabrication tool that is able to synthesize multifunctional fiber-optic tip devices with potentially high throughput capability, especially if suitable strategies are devised to efficiently parallelize the self-assembling stage.

To analyze the physics underlying the fabricated sensing probes, we developed a numerical tool that is able to study arbitrary structures on optical fiber tips by taking into account both the field distribution of the fundamental mode in a single-mode optical fiber and the finite size of the crystal structure illuminated though the fiber tip. The results of the full-wave numerical analysis have been found to be in good agreement with the experimental data and revealed that the fabricated sensing probes act as structured two-beam interferometers where a complex interplay occurs between the classical optical interference mechanism and the plasmonic excitation occurring at the metallic interfaces. To show the functionalities of the realized optical probes, we investigated the sensing performances in terms of sensitivity to the SRI. The fabricated sensing probes revealed impressive performances with sensitivities as high as 2000 nm/RIU

Although complete understanding has not yet been achieved, basic considerations of the experimental data indicate that the interplay between the different effects provides sensitivity

values typically observed in SPR devices with larger metallic areas.[4] In our case, these extremely high sensitivity values are achieved with active regions (fiber tip area 0.012 mm^2) that are typically used for LPSR devices with sensitivity values that do not exceed a few hundred nm/RIU.[2,4]

The experimental results demonstrate the feasibility of the proposed technological approach to attain advanced miniaturized sensors by exploiting an easy and low-cost fabrication process, which is suitable for rapid prototyping and mass production.

METHODS

Numerical Section. *Details of the Optical-Fiber-Based Model.* The simulations were carried out via FEM using the commercial modeling tool COMSOL Multiphysics - RF Module (COMSOL Inc., Burlington, MA, USA).

To determine the reflectance of arbitrary metal−dielectric structures on the tip of a single-mode optical fiber, we calculated the scattering parameters of the structure under investigation by properly defining the computation domain and the boundary conditions.

The computational domain is composed of a modified optical fiber, containing a core with a diameter of 9 μm and a reduced cladding with a diameter of 16 μm and terminated with a perfect electric conductor (PEC). The core and cladding refractive indexes are 1.46 and 1.455, respectively. The physical and geometrical features of this modified optical fiber have been chosen to make the optical fiber "single-mode" with a Gaussian-like mode, then used as a source to keep the computational domain as small as possible. The metallo-dielectric structure to be simulated is drawn on the optical fiber tip, followed by a layer of air, which represents the surrounding medium. The refractive index of polystyrene is 1.58 over the entire spectral range. Both losses and the dispersion of gold have been taken into account.[23]

To reduce the computational burden, the entire structure is reduced to one-quarter of its original size by applying PEC and perfectly magnetic-conducting boundary conditions. This further reduction of the computational domain implies that the structure under investigation must have mirror symmetry.

On the curved boundary surface, we assumed a scattering boundary condition to make the boundary transparent to scattered waves. The bottom and top boundaries are the input and output ports for the *S*-parameter calculations. At the input, a Gaussian-like source is set to 1 W.

The simulations were performed on a workstation with an i7 CPU 3.47 GHz and 24 GB RAM.

Experimental Section. *Spectral Characterizations.* The spectral reflectance measurements were carried out by illuminating the fiber tip with a broadband optical source (covering the wavelength range 1250−1650 nm) and redirecting the reflected light (via a 2 × 1 directional coupler) to an optical spectrum analyzer (Ando AQ6317C). In addition, to compensate for intensity fluctuations of the source versus wavelength, the sample reflectance was normalized using a fiber-optic reference mirror fabricated by depositing a 160 nm thick gold film on the tip of a standard single-mode fiber. The schematic of the characterization setup is reported in Figure S8 in the Supporting Information.

ASSOCIATED CONTENT

Supporting Information

This material is available free of charge via the Internet at http://pubs.acs.org.

AUTHOR INFORMATION

Corresponding Authors

*E-mail (M. Giordano): gmichele@unina.it.
*E-mail (A. Cusano): a.cusano@unisannio.it.

Author Contributions

⊥M. Pisco and F. Galeotti contributed equally to this work.

Notes

The authors declare no competing financial interest.

REFERENCES

(1) Homola, J. Surface Plasmon Resonance Sensors for Detection of Chemical and Biological Species. *Chem. Rev.* **2008**, *108*, 462−493.
(2) Stewart, M. E.; Anderton, C. R.; Thompson, L. B.; Maria, J.; Gray, S. K.; Rogers, J. A.; Nuzzo, R. G. Nanostructured Plasmonic Sensors. *Chem. Rev.* **2008**, *108*, 494−521.
(3) Homola, J.; Koudela, I.; Yee, S. S. Surface Plasmon Resonance Sensors Based on Diffraction Gratings and Prism Couplers: Sensitivity Comparison. *Sensor Actuators B: Chem.* **1999**, *54*, 16−24.
(4) Roh, S.; Chung, T.; Lee, B. Overview of the Characteristics of Micro- and Nano-Structured Surface Plasmon Resonance Sensors. *Sensors-Basel* **2011**, *11*, 1565−1588.
(5) Lee, B.; Roh, S.; Park, J. Current Status of Micro- and Nano-Structured Optical Fiber Sensors. *Opt. Fiber Technol.* **2009**, *15*, 209−221.
(6) Srivastava, S. K.; Gupta, B. D. Fiber Optic Plasmonic Sensors: Past, Present and Future. *Open Opt. J.* **2013**, *7*, 58−83.
(7) Sharma, A. K.; Gupta, B. D. Fibre-Optic Sensor Based on Surface Plasmon Resonance with Ag-Au Alloy Nanoparticle Films. *Nanotechnology* **2006**, *17*, 124−131.
(8) Kanso, M.; Cuenot, S.; Louarn, G. Sensitivity of Optical Fiber Sensor Based on Surface Plasmon Resonance: Modeling and Experiments. *Plasmonics* **2008**, *3*, 49−57.
(9) Verma, R. K.; Sharma, A. K.; Gupta, B. D. Surface Plasmon Resonance Based Tapered Fiber Optic Sensor with Different Taper Profiles. *Opt. Commun.* **2008**, *281*, 1486−1491.
(10) Lin, H. Y.; Huang, C. H.; Cheng, G. L.; Chen, N. K.; Chui, H. C. Tapered Optical Fiber Sensor Based on Localized Surface Plasmon Resonance. *Opt Express* **2012**, *20*, 21693−21701.
(11) Srivastava, S. K.; Arora, V.; Sapra, S.; Gupta, B. D. Localized Surface Plasmon Resonance-Based Fiber Optic U-Shaped Biosensor for the Detection of Blood Glucose. *Plasmonics* **2012**, *7*, 261−268.
(12) Schuster, T.; Herschel, R.; Neumann, N.; Schaffer, C. G. Miniaturized Long-Period Fiber Grating Assisted Surface Plasmon Resonance Sensor. *J. Lightwave Technol.* **2012**, *30*, 1003−1008.
(13) Chiu, M.-H.; Shih, C.-H.; Chi, M.-H. Optimum Sensitivity of Single-Mode D-Type Optical Fiber Sensor in the Intensity Measurement. *Sens. Actuators, B* **2007**, *123*, 1120−1124.
(14) Hautakorpi, M.; Mattinen, M.; Ludvigsen, H. Surface-Plasmon-Resonance Sensor Based on Three-Hole Microstructured Optical Fiber. *Opt. Express* **2008**, *16*, 8427−8432.
(15) Yu, X.; Zhang, Y.; Pan, S. S.; Shum, P.; Yan, M.; Leviatan, Y.; Li, C. M. A Selectively Coated Photonic Crystal Fiber Based Surface Plasmon Resonance Sensor. *J. Opt. (UK)* **2010**, *12*, 015005.
(16) Grunwald, B.; Holst, G. Fibre Optic Refractive Index Microsensor Based on White-Light Spr Excitation. *Sensor Actuators, A: Phys.* **2004**, *113*, 174−180.
(17) Suzuki, H.; Sugimoto, M.; Matsui, Y.; Kondoh, J. Effects of Gold Film Thickness on Spectrum Profile and Sensitivity of a Multimode-Optical-Fiber Spr Sensor. *Sensor Actuators, B: Chem.* **2008**, *132*, 26−33.
(18) Hutter, E.; Fendler, J. H. Exploitation of Localized Surface Plasmon Resonance. *Adv. Mater.* **2004**, *16*, 1685−1706.

(19) Lin, Y. B.; Zou, Y.; Mo, Y. Y.; Guo, J. P.; Lindquist, R. G. E-Beam Patterned Gold Nanodot Arrays on Optical Fiber Tips for Localized Surface Plasmon Resonance Biochemical Sensing. *Sensors (Basel)* **2010**, *10*, 9397−9406.
(20) Lin, Y. B.; Zou, Y.; Lindquist, R. G. A Reflection-Based Localized Surface Plasmon Resonance Fiber-Optic Probe for Biochemical Sensing. *Biomed. Opt. Express* **2011**, *2*, 478−484.
(21) Dhawan, A.; Gerhold, M. D.; Muth, J. F. Plasmonic Structures Based on Subwavelength Apertures for Chemical and Biological Sensing Applications. *IEEE Sens. J.* **2008**, *8*, 942−950.
(22) Dhawan, A.; Muth, J. F.; Leonard, D. N.; Gerhold, M. D.; Gleeson, J.; Vo-Dinh, T.; Russell, P. E. Focused in Beam Fabrication of Metallic Nanostructures on End Faces of Optical Fibers for Chemical Sensing Applications. *J. Vac. Sci. Technol. B* **2008**, *26*, 2168−2173.
(23) Consales, M.; Ricciardi, A.; Crescitelli, A.; Esposito, E.; Cutolo, A.; Cusano, A. Lab-on-Fiber Technology: Toward Multifunctional Optical Nanoprobes. *ACS Nano* **2012**, *6*, 3163−3170.
(24) Consales, M.; Pisco, M.; Cusano, A. Lab-on-Fiber Technology: A New Avenue for Optical Nanosensors. *Photonic Sens.* **2012**, *2*, 289−314.
(25) Kostovski, G.; Stoddart, P. R.; Mitchell, A. The Optical Fiber Tip: An Inherently Light-Coupled Microscopic Platform for Micro- and Nanotechnologies. *Adv. Mater.* **2014**, DOI: 10.1002/adma.201304605.
(26) Smythe, E. J.; Dickey, M. D.; Whitesides, G. M.; Capasso, F. A Technique to Transfer Metallic Nanoscale Patterns to Small and Non-Planar Surfaces. *ACS Nano* **2009**, *3*, 59−65.
(27) Smythe, E. J.; Dickey, M. D.; Bao, J. M.; Whitesides, G. M.; Capasso, F. Optical Antenna Arrays on a Fiber Facet for in Situ Surface-Enhanced Raman Scattering Detection. *Nano Lett.* **2009**, *9*, 1132−1138.
(28) Lipomi, D. J.; Martinez, R. V.; Kats, M. A.; Kang, S. H.; Kim, P.; Aizenberg, J.; Capasso, F.; Whitesides, G. M. Patterning the Tips of Optical Fibers with Metallic Nanostructures Using Nanoskiving. *Nano Lett.* **2011**, *11*, 632−636.
(29) Stoddart, P. R.; White, P. A.; Mazzolini, A. Chemical Sensors Based on Nanoparticle Arrays. In *Proceedings of the International Symposium on Smart Materials, Nano- and Micro-Systems*; Melbourne, Victoria, Australia, Dec 16−18, 2002, Vol. 4934; 2002, SPIE,2002; pp 61−69.
(30) Yap, F. L.; Thoniyot, P.; Krishnan, S.; Krishnamoorthy, S. Nanoparticle Cluster Arrays for High-Performance Sers through Directed Self-Assembly on Flat Substrates and on Optical Fibers. *ACS Nano* **2012**, *6*, 2056−2070.
(31) Andrade, G. F. S.; Fan, M. K.; Brolo, A. G. Multilayer Silver Nanoparticles-Modified Optical Fiber Tip for High Performance SERS Remote Sensing. *Biosens. Bioelectron.* **2010**, *25*, 2270−2275.
(32) Yan, H. T.; Wang, M.; Ge, Y. X.; Yu, P. Colloidal Crystals Self-Assembled on the End Face of Fiber: Fabrication and Characterizations. *Opt. Fiber Technol.* **2009**, *15*, 324−327.
(33) Pisco, M.; Quero, G.; Iadicicco, A.; Giordano, M.; Galeotti, F.; Cusano, A. Lab on Fiber by Using the Breath Figure Technique. *Proc. SPIE 8774, Opt. Sens.* **2013**, *2013*, 87740R.
(34) Escalé, P.; Rubatat, L.; Billon, L.; Save, M. Recent Advances in Honeycomb-Structured Porous Polymer Films Prepared via Breath Figures. *Eur. Polym. J.* **2012**, *48*, 1001−1025.
(35) Hernandez-Guerrero, M.; Stenzel, M. H. Honeycomb Structured Polymer Films via Breath Figures. *Polym. Chem. (UK)* **2012**, *3*, 563−577.
(36) Ma, H. M.; Hao, J. C. Ordered Patterns and Structures via Interfacial Self-Assembly: Superlattices, Honeycomb Structures and Coffee Rings. *Chem. Soc. Rev.* **2011**, *40*, 5457−5471.
(37) Bolognesi, A.; Mercogliano, C.; Yunus, S.; Civardi, M.; Comoretto, D.; Turturro, A. Self-Organization of Polystyrenes into Ordered Microstructured Films and Their Replication by Soft Lithography. *Langmuir* **2005**, *21*, 3480−3485.
(38) Srinivasarao, M.; Collings, D.; Philips, A.; Patel, S. Three-Dimensionally Ordered Array of Air Bubbles in a Polymer Film. *Science* **2001**, *292*, 79−83.
(39) Stenzel, M. H.; Barner-Kowollik, C.; Davis, T. P. Formation of Honeycomb-Structured, Porous Films via Breath Figures with Different Polymer Architectures. *J. Polym. Sci. Polym. Chem.* **2006**, *44*, 2363−2375.
(40) Haupt, M.; Miller, S.; Sauer, R.; Thonke, K.; Mourran, A.; Moeller, M. Breath Figures: Self-Organizing Masks for the Fabrication of Photonic Crystals and Dichroic Filters. *J. Appl. Phys.* **2004**, *96*, 3065−3069.
(41) Yabu, H.; Hirai, Y.; Matsuo, Y.; Ijiro, K.; Shimomura, M. Double-Layered Metal Mesh Film with Limited Viewing Angle Prepared by Electroless Plating of Self-Organized Honeycomb Film. *Macromol. Symp.* **2008**, *267*, 100−104.
(42) Yabu, H.; Shimomura, M. Single-Step Fabrication of Transparent Superhydrophobic Porous Polymer Films. *Chem. Mater.* **2005**, *17*, 5231−5234.
(43) Galeotti, F.; Calabrese, V.; Cavazzini, M.; Quici, S.; Poleunis, C.; Yunus, S.; Bolognesi, A. Self-Functionalizing Polymer Film Surfaces Assisted by Specific Polystyrene End-Tagging. *Chem. Mater.* **2010**, *22*, 2764−2769.
(44) Galiatsatos, V. Refractive Index, Stress-Optical Coefficient, and Optical Configuration Parameter of Polymers. In *Physical Properties of Polymers Handbook*, second ed.; Springer: New York, 2007; pp 823−853.
(45) Yamazaki, H.; Ito, K.; Yabu, H.; Shimomura, M. Formation and Control of Line Defects Caused by Tectonics of Water Droplet Arrays during Self-Organized Honeycomb-Patterned Polymer Film Formation. *Soft Matter* **2014**, *10*, 2741−2747.
(46) Limaye, A. V.; Narhe, R. D.; Dhote, A. M.; Ogale, S. B. Evidence for Convective Effects in Breath Figure Formation on Volatile Fluid Surfaces. *Phys. Rev. Lett.* **1996**, *76*, 3762−3765.
(47) Ricciardi, A.; Pisco, M.; Gallina, I.; Campopiano, S.; Galdi, V.; O' Faolain, L.; Krauss, T. F.; Cusano, A. Experimental Evidence of Guided-Resonances in Photonic Crystals with Aperiodically Ordered Supercells. *Opt. Lett.* **2010**, *35*, 3946−3948.
(48) Ricciardi, A.; Pisco, M.; Cutolo, A.; Cusano, A.; Faolain, L. O.; Krauss, T. F.; Castaldi, G.; Galdi, V. Evidence of Guided Resonances in Photonic Quasicrystal Slabs. *Phys. Rev. B* **2011**, *84*, 085135.
(49) Fan, S. H.; Joannopoulos, J. D. Analysis of Guided Resonances in Photonic Crystal Slabs. *Phys. Rev. B* **2002**, *65*, 235112.
(50) Stockman, M. I. Nanoplasmonics: Past, Present, and Glimpse into Future. *Opt. Express* **2011**, *19*, 22029−22106.
(51) Stewart, M. E.; Mack, N. H.; Malyarchuk, V.; Soares, J. A. N. T.; Lee, T.-W.; Gray, S. K.; Nuzzo, R. G.; Rogers, J. A. Quantitative Multispectral Biosensing and 1d Imaging Using Quasi-3d Plasmonic Crystals. *Proc. Natl. Acad. Sci. U.S.A.* **2006**, *103*, 17143−17148.
(52) Cao, J.; Galbraith, E. K.; Sun, T.; Grattan, K. T. V. Comparison of Surface Plasmon Resonance and Localized Surface Plasmon Resonance-Based Optical Fibre Sensors. *J. Phys. Conf. Ser.* **2011**, *307*.
(53) Orfanidis, S. J. *Electromagnetic Waves and Antennas*; Rutgers Univ. Press: New Brunswick, NJ. Available online: http://www.ece.rutgers.edu/~orfanidi/ewa/.
(54) Sihvola, A. Mixing Rules with Complex Dielectric Coefficients. *Subsurf. Sens. Technol. Appl.* **2000**, *1*, 393−415.
(55) Ricciardi, A.; Consales, M.; Quero, G.; Crescitelli, A.; Esposito, E.; Cusano, A. Versatile Optical Fiber Nanoprobes: From Plasmonic Biosensors to Polarization-Sensitive Devices. *ACS Photonics* **2013**, *1*, 69−78.